Penalty-Based Interface Technology for Prediction of Delamination Growth in Laminated Structures

FINAL REPORT

Submitted to:

NASA Langley Research Center
NASA Contract Number: NAG-1-2213

By:

Ronald C. Averill
Department of Mechanical Engineering
Michigan State University
East Lansing, MI 48824-1226
MSU Contract Number: 61-2770

Executive Summary

An effective interface element technology has been developed for connecting and simulating crack growth between independently modeled finite element subdomains (e.g., composite plies). This method has been developed using penalty constraints and allows coupling of finite element models whose nodes do not necessarily coincide along their common interface. Additionally, the present formulation leads to a computational approach that is very efficient and completely compatible with existing commercial software. The present interface element has been implemented in the commercial finite element code ABAQUS as a User Element Subroutine (UEL), making it easy to test the approach for a wide range of problems. The interface element technology has been formulated to simulate delamination growth in composite laminates. Thanks to its special features, the interface element approach makes it possible to release portions of the interface surface whose length is smaller than that of the finite elements. In addition, the penalty parameter can vary within the interface element, allowing the damage model to be applied to a desired fraction of the interface between the two meshes. Results for double cantilever beam DCB, end-loaded split (ELS) and fixed-ratio mixed mode (FRMM) specimens are presented. These results are compared to measured data to assess the ability of the present damage model to simulate crack growth.

1. INTRODUCTION

With model sharing and large scale analysis activities on the rise, there is an increasing need to perform a unified analysis of a structural assembly using sub-structural models created independently. These sub-structural models are frequently created by different engineers using different software and in different geographical locations, with little or no communication between the teams of engineers creating the models. As a result, these models are likely to be incompatible at their interfaces, making it very difficult to combine them for a unified analysis of the entire assembly. Finite element interface technology has been developed to facilitate the joining of independently modeled substructures.

Unconventional approaches have been employed to connect special elements based on analytical solutions to finite element models (Aminpour et al., 1991; Jinping et al., 1991). In order to take advantage of parallel computing, Farhat et al. (1991,1992) developed a domain decomposition approach. In another work (Maday et al., 1988) non-conforming "mortar" elements are employed to connect incompatible subdomains. The finite element interface technology developed at NASA LaRC (Ransom et al., 1993, 1997; Housner et al., 1995, Aminpour et al., 1995, 1997) and elsewhere (Aminpour et al., 1998) allows the connection of independently modeled substructures with incompatible discretization along the common boundary. This approach has matured to a point that it is now very effective. However, because this form of the interface technology utilizes Lagrange multipliers to enforce the interface constraint conditions, the resulting system of equations is not positive-definite. Recently, an alternative formulation for the finite element interface technology based on Lagrange multipliers has been developed (Aminpour et al., 2000). The alternative approach recasts the interface element constraint equations in the form of multi-point constraints. This change allows an easier implementation of the formulation in a standard finite element code and alleviates the issues related to the resulting non-positive definite system of equations. The method seems to provide reliable results, but the formulation of the interface method is still quite complicated.

A possible remedy for these shortcomings is to modify the existing hybrid variational formulation of the interface element by enforcing the interface constraints via a penalty method as opposed to the current Lagrange multiplier approach. The primary consequences of this modification will be (i) a simple formulation that is easily implemented in commercial finite elements codes, (ii) a positive-definite and banded stiffness matrix and (iii) a reduced number of DOFs, since the Lagrange multiplier degrees of freedom (DOFs) will not be present. Thus, the penalty approach should greatly enhance the computational efficiency of the interface element technology.

From an accuracy point of view, the penalty method enforces the constraints only approximately, depending on the value of the penalty parameter chosen, while the Lagrange multiplier approach enforces the constraints exactly. The penalty method interface approach was recently attempted using a single global value of the penalty parameter to enforce all constraints (Cho et al., 1998). This study demonstrated the validity and the effectiveness of the penalty approach in an interface element. However, there is need for specific guidelines regarding the

selection of an appropriate value of the penalty parameter, especially when the substructures to be connected have different material and/or section stiffnesses. A criterion for choosing the penalty parameter in the framework of the interface element under investigation has been developed by the authors (Pantano and Averill, 2002a-2002b).

Though the penalty-based interface element was originally developed to "connect" two regions of a finite element mesh, it can also be used effectively to simulate crack growth, such as delamination. Initiation and evolution of the delamination may be predicted by a fracture mechanics approach or by interlaminar strength, introducing an interface constitutive law between the layers.

The fracture mechanics approach uses strain energy release rate G as a parameter for assessing delamination, initiation and growth. In the fracture mechanics approach, strain energy release rate per unit area delaminated is evaluated and compared with the critical strain energy release rate G_c. Thus, much attention has been given to correctly evaluating strain energy release rate. Pradhan and Tay (1998), Kaczmarek et al. (1998), Rinderknecht and Kroplin (1997), Wang and Raju (1996), Raju et al. (1996), Hwu et al. (1995), Hitchings et al. (1996), developed finite element approaches for the analysis of delamination growth in composite plates based on the virtual crack closure technique (VCCT) to compute the total energy release rate G, including contribution by all the three modes.

In the strength of materials approach, the local state of stress at the interface is compared with relevant interface strengths. Use of finite element analysis makes the strength of materials approach attractive, as the stresses can be evaluated quickly and efficiently, and interlaminar stresses can be easily compared with the measured strengths. However, unless delamination initiation is the only concern, failure criteria usually combine strength of materials features with fracture mechanics ones. Since the cohesive zone can still transfer load after the onset of damage, a softening model is required that describes how the stiffness is gradually reduced to zero after the interfacial stress exceeds the interlaminar tensile strength. Reliable prediction of the softening behavior can be obtained by relating the work of separation to the critical value of the strain energy release rate G_c. At a given point on the interface, the area under the stress-relative displacement curve is equal to G_c. This approach to the determination of the delamination growth has been adopted by Reedy et al. (1997), Davila et al. (2001), Mi et al. (1998), Chen et al. (1999), Alfano et al. (2001), Lammerant and Verpoest (1996), Schellekens and de Borst (1993), Schipperen and Lingen (1999), and Moorthy and Reddy (1999). Interface elements are introduced to connect the individual plies of a composite laminate, but the way this connection is realized can differ. Two approaches can be identified: point to point interface elements acting like springs which connect pairs of nodes, and continuous interface elements that connect pairs of two or three dimensional finite elements.

In the work of Allix and Corigliano (1999), Point and Sacco (1996), Ladevèze (1992), Bottega (1983), a constitutive law for the interface material, able to handle the delamination phenomenon, has been obtained starting from an adhesion model and is based on the definition of a damaged strain energy density in the interface layer. Chakraborty and Pradhan (1999) performed a fully 3D finite element analysis to study delamination at the interface of graphite/epoxy and glass/epoxy laminates with broken central plies. Their methodology for predicting delamination employs simultaneously strength and fracture mechanics approaches. Joo and Sun (1994), Ko et al. (1992), Mohammadi et al. (1998), Zhao et al. (1999) and Chang

and Springer (1986) predicted delamination initiation by a strength approach very similar to the one of Chakraborty and Pradhan (1999). A three-dimensional finite-deformation cohesive element and a class of irreversible cohesive laws was developed by Ortiz and Pandolfi (1999) and Pandolfi et al. (1999). Moes et al. (1999) presented an innovative finite element able to account for crack growth inside the element. The approach adopted for delamination initiation and growth is based upon the maximum circumferential stress criterion. Stresses are computed by the classical fracture mechanics equation for the stress distribution at the crack tip. This finite element type of approach, also referred to as *singularity element* approach, was also used by Aminpour and Hosapple (1991) and Lee and Gao (1995).

This report will briefly review the penalty-based interface element technology and subsequently introduce a new application of the interface element for predicting delamination crack growth in laminated structures.

2. GENERAL DESCRIPTION OF THE INTERFACE ELEMENT

Consider two independently modeled subdomains Ω_1 and Ω_2 as shown in Figure 1(a) and 1(b), respectively, for a 2D and for a 3D geometry. The two substructures are connected to each other using an interface element acting like "glue" at the common interface. The interface element is discretized with a set of nodes that are independent of the nodes at the interface in subdomains Ω_1 and Ω_2. The coupling terms associated to the interface element are arranged in the form of a "stiffness" matrix and assembled with the other finite element stiffness matrices as usual.

The nodal displacements of the sub-domain Ω_j are identified by q_j^o and q_j^i. The superscript *o* marks the degrees of freedom (DOFs) that are not on the interfaces, while *i* denotes DOFs that are on the interfaces. The interface displacement field u_j of the sub-domain Ω_j is expressed in terms of the unknown nodal displacements q_j^i. The displacement field V is approximated on the entire interface element surface in terms of unknown nodal displacements q_s.

$$u_j = N_j q_j^i \qquad V = T q_s \tag{1}$$

where N_j can be the matrices of linear Lagrange interpolation functions and T is a matrix of cubic spline interpolation functions. In the penalty interface method the displacement continuity constraint is imposed in a least squares sense using two vectors of penalty parameters γ_1 and γ_2. Thus the total potential energy of the system assumes the form:

$$\pi = \pi_{\Omega_1} + \pi_{\Omega_2} + \frac{\gamma_1}{2}\int_S (V - u_1)^2\, ds + \frac{\gamma_2}{2}\int_S (V - u_2)^2\, ds \tag{2}$$

The equilibrium configuration is found by taking the first variation of π respect to all the DOFs, but not the vectors of penalty parameters γ_1 and γ_2, which are predetermined constants.

$$\delta\pi\big|_{q_1^o, q_1^i, q_S, q_2^o, q_2^i} = 0 \tag{3}$$

The global system of equations of the penalty hybrid interface method assumes the following form:

$$\begin{bmatrix} K_1^{oo} & K_1^{oi} & 0 & 0 & 0 \\ K_1^{io} & K_1^{ii}+G_1^{ii} & -G_1^{is} & 0 & 0 \\ 0 & -G_1^{si} & G_1^{ss}+G_2^{ss} & -G_2^{si} & 0 \\ 0 & 0 & -G_2^{is} & K_2^{ii}+G_2^{ii} & K_2^{io} \\ 0 & 0 & 0 & K_2^{oi} & K_2^{oo} \end{bmatrix} \begin{Bmatrix} q_1^o \\ q_1^i \\ q_s \\ q_2^i \\ q_2^o \end{Bmatrix} = \begin{Bmatrix} f_1^o \\ f_1^i \\ 0 \\ f_2^i \\ f_2^o \end{Bmatrix} \tag{4}$$

where:

$$G_j^{ii} = \gamma_j \int_s (N_j^T N_j) ds \,,\; G_j^{is} = \gamma_j \int_s (N_j^T T_j) ds \,,\; G_j^{si} = \left[G_j^{is}\right]^T \,,\; G_j^{ss} = \gamma_j \int_s (T_j^T T_j) ds \tag{5}$$

This is a symmetric, banded and positive definite (after boundary conditions are imposed) global stiffness matrix. The "stiffness" matrix and generalized vector of unknown displacements associated with the interface element can be defined as:

$$\begin{bmatrix} G_1^{ii} & -G_1^{is} & 0 \\ -G_1^{si} & G_1^{ss}+G_2^{ss} & -G_2^{si} \\ 0 & -G_2^{is} & G_2^{ii} \end{bmatrix} \begin{Bmatrix} q_1^i \\ q_s \\ q_2^i \end{Bmatrix} = \begin{Bmatrix} 0 \\ 0 \\ 0 \end{Bmatrix} \tag{6}$$

For a detailed description of the interface element formulation, see Pantano and Averill (2002a-2002b).

3. DETERMINATION OF THE PENALTY PARAMETERS

In the penalty method, the displacement continuity constraint is imposed through penalty parameters, a set of predetermined constants. The FE solution obtained using this method is approximate, with its accuracy depending on the value of the adopted penalty parameters. It is known that the penalty parameter should depend on the material and/or geometric properties of the two sub-regions being joined. Further, there is a relationship between the penalty parameter and the Lagrange multiplier that enforces a given constraint. The Lagrange multiplier method imposes the continuity constraint exactly; thus it defines the upper limit to the accuracy of the penalty method. Knowledge of the correct solution for simple model problem facilitates relating the value of the penalty parameter to the geometrical and material properties of the model under consideration. In our pursuit of the proper penalty parameter values, a variety of one and two-dimensional problems have been studied with both the Lagrange multiplier method and the penalty method. The types of finite elements that have been investigated are: conventionally formulated and reduced integrated Timoshenko beam elements, plane stress quadrilateral elements and plate elements based on the first order shear deformation theory (FSDT), or Mindlin plate theory. For each finite element formulation, different penalty parameters are associated to the various nodal DOFs. For example, the Timoshenko beam element has three independent nodal DOFs: the axial displacement u, the transverse displacement w and the

rotation ψ. Thus, three different penalty parameters γ_u, γ_w and γ_ψ are employed to enforce the interface continuity constraints on the DOFs u, w and ψ. An independent choice of the penalty parameters is necessary since each degree of freedom can be related differently to the material and geometric properties of the finite element model.

The methodology adopted in finding the relations will now be described. First the most common load cases for the FE type under consideration are applied separately to a simple model of one or two elements. The formulations and solutions are obtained using both the Lagrange multiplier method and the penalty method. The displacement solutions from the two methods are compared individually for each degree of freedom. The ratio between the two solutions is expressed in the form:

$$\frac{u^{penalty}}{u^{Lagrange}} = 1 + \frac{f}{\gamma} \tag{7}$$

where $f = f$(element geometric properties, material properties, and loads).

Once this simple expression has been identified, the penalty parameter γ is set equal to: $\gamma = \beta f$. Then, the ratio between the solutions becomes independent of material and geometrical properties:

$$\frac{u^{penalty}}{u^{Lagrange}} = 1 + \frac{1}{\beta} \tag{8}$$

The accuracy of the solution depends directly on the value assigned to the parameter β. The degree of precision of the solution cannot be indefinitely increased, since round off amplification error would rise. However, once a reasonable compromise between constraint representation error and the round off error has been evaluated, a value of β can be identified that is able to produce the same level of accuracy for every combination of material and geometrical properties.

For a detailed description of the determination of the penalty parameter values, see Pantano and Averill (2002a-2002b).

4. INTERFACE TECHNOLOGY FOR MODELING DELAMINATION

The interface element technology (Pantano and Averill, 2002a-2002b) was originally developed for the purpose of connecting independently modeled subdomains. By taking the converse view, it should be possible to use this technology to disconnect two regions of a model during crack growth. In this context, the present interface element approach would have several advantages over the conventional FE one. For example, the present approach is able to release arbitrary portions of the interface that are smaller than the finite element length, thereby determining the crack advance. This can be achieved by changing the extreme values of the interval of integration of the interface element or by reducing the value of the penalty parameter for a part of that interval. Within each interface sub-region it is possible to evaluate forces at the

interface and to reduce the value of the penalty parameter as needed. Thus, it is possible to overcome a limitation common to the delamination techniques found in the literature, which require delamination growth to be simulated in a discretized form by releasing nodes or elements of the FE model.

The damage model implemented in the developed interface element is one that is commonly adopted (Reedy et al., 1997; Davila et al., 2001; Mi et al., 1998; Chen et al., 1999; Alfano et al., 2001; Lammerant and Verpoest, 1996; Schellekens and de Borst, 1993; Schipperen and Lingen, 1999; Moorthy and Reddy, 1999). It mixes features of strength of materials approaches and fracture mechanics. A bilinear softening model has been implemented in the present model (see Figure 2). In single-mode delamination, as the load is progressively increased, the relative displacement δ the two subdomains FE meshes grows proportionally according to the value of the penalty stiffness γ. When δ_0 is reached the stress is equal to the interfacial tensile strength σ_t, the maximum stress level possible. For higher relative displacements the interface accumulates damage and its ability to sustain stress decreases progressively. Once δ exceeds δ_F the interface is fully debonded and it is no longer able to support any stress. If the load were removed after δ_0 has been exceeded but before δ_F has been reached, the model would unload to the origin. For example, if after reaching point K (see Figure 2) the load is reduced, the model unloads along the line KO. If the load is reapplied, the stress grows with the relative displacement along the same line KO.

This behavior is obtained by an effective reduction in the penalty stiffness γ. In the present model, a new parameter D is introduced in order to signify the damage accumulated at the interface:

$$\sigma = (1-D)\gamma\delta \tag{9}$$

Thus D is a damage parameter, whose initial value is zero. D starts growing when $\delta \geq \delta_0$ and reaches the value 1 when $\delta \geq \delta_F$.

The value of D is computed from geometry to be:

$$D(\delta) = \frac{\delta_F(\delta - \delta_0)}{\delta(\delta_F - \delta_0)} \tag{10}$$

The interfacial constitutive model is entirely defined when any two of the following properties are known: G_c, σ_t, δ_0 and δ_F, where G_c is the critical strain energy release rate, which is equal to the area under σ-δ curve in Figure 2. The following two relations exist among these parameters:

$$G_c = \frac{\delta_F \sigma_t}{2} \tag{11}$$

$$\delta_0 = \frac{\sigma_t}{\gamma} \tag{12}$$

The bilinear interface model is applied to a sub-region of the interface between the two meshes; the smaller is the length of each sub-region the higher is the accuracy of the prediction. A conventional implementation of the discussed damage technique requires the model to be applied along the length of one finite element, wherein the crack can advance in a discrete way

only by failing one element at a time. Both limitations necessitate the use of a refined finite element mesh. Using the interface element previously presented, the damage evolution scheme in our model is effectively mesh-independent, wherein continuity between sub-regions of the interface that are much smaller than the finite element length can be released.

Note that different softening interface laws can be implemented in the present approach. In Figure 3 some of the most commonly used damage models are reported. If a damage model different from the bilinear one is adopted, the expression (10), which allows the evaluation of damage parameter D as a function of the relative displacement δ, must be modified. The changes in the relation (10) will easily follow from the new geometry of the softening interface model.

Thus, the present interface model can be applied to a desired fraction of the interface between the two meshes. If we divide the interface element into a given number of intervals n, each of them will obey the rules of the failure model independently from the others. This corresponds to changing the total potential energy of the system in the following way:

$$\pi = \pi_{\Omega_1} + \pi_{\Omega_2} + \frac{1}{2}\sum_{i=1}^{n}(1-D_i)\gamma_1 \int_{L_{i-1}}^{L_i} (V-u_1)^2\, ds + \sum_{i=1}^{n}(1-D_i)\gamma_2 \int_{L_{i-1}}^{L_i} (V-u_2)^2\, ds \qquad (13)$$

where D_i is the damage parameter associated with the interval i, and the interval i is defined over the range (L_{i-1}, L_i). L_i is the value of the interface coordinate L at the end of the i^{th} interval. The value of the relative displacement δ is evaluated at the center of the interval i. By allowing crack advance in a more continuous way, a higher accuracy of the simulation can be achieved.

To illustrate this concept, consider the two incompatible meshes shown in Figure 4. They are joined by two interface elements whose length equals that of five conventional elements of the top mesh and four elements of the bottom mesh. Two forces F applied at the tip are responsible for effecting a mode I stress field at the interface. The interface element at the crack tip is shown in Figure 4(a) as divided in ten intervals. The intervals do not need to match any of the nodes in the upper or lower mesh, but in this example some of them coincide. Moreover, the number of intervals in the interface element is a parameter that can be changed as desired. Following the progression in Figure 4, a simulation of the delamination growth is achieved by releasing portions (intervals) of the interface element. In Figure 4(b), the first interval is failed. The portion of the interface element not released still applies its constraint to the lower and upper elements next to the crack tip.

In Figure 4(c) the second interval is failed, which determines the complete release of the element on the upper mesh near the crack tip. The element on the lower mesh moves downward too, but being still held in part, the movement is small. The next advance in the crack length, Figure 4(d), frees the lower element and only partially the upper. Figure 4(e) shows the effect of releasing yet another interval. Similarly, when all the intervals are failed the FE model behaves as though the first interface element is not present. Then, the next interface element starts failing. In this example, intervals whose length is half of the smaller finite element extension have been used. Dividing the interface element into more intervals or reducing its length would improve the accuracy of the model.

By progressively reducing the dimension of the intervals in which the interface element is divided, the results will converge to a values that will not change noticeably as the intervals

length are further reduced. Usually, this kind of convergence study do not require several simulations since the rate of convergence is typically high. Moreover, experience in choosing the intervals length developed by working with similar simulations can be easily applied to new calculations. It needs to be underlined that intervals dimensions smaller than the minimum element size along the crack should not be used as the accuracy will quickly be reduced. In the numerical results convergence of the solution with the number of intervals is investigated for the double cantilever beam DCB specimen.

The other essential convergence study, which is commonly necessitated in FE approaches to the simulations of crack growth, is based on investigating the model behavior as a function of the number of increments in which the given load/displacement is progressively applied. At the beginning of each increments, or load step, the relative displacement δ at the center of the interval is obtained from the FE calculation for all the intervals in which the interface element is divided. If the increment in the applied load or displacement is too high, the bilinear softening model cannot work correctly and the results will be incorrect. For example, if at the beginning of the increment the relative displacement δ for the interval at the crack tip is slightly smaller than δ_0 while at the end of the increment it is much higher, for the entire load step the damage parameter D maintain its zero value and the stress at the interface will considerably exceed the interfacial tensile strength σ_t. The softening will be applied only in the next increment, with the additional flawed consequence that when the interval will fail the area under σ-δ curve will be higher than the critical strain energy release rate G_c. Thus, as for the great majority of the FE approaches to the simulations of crack growth, a convergence study on the number of increments should always be performed. In the numerical results convergence of the solution with the number of increments is reported for the double cantilever beam DCB specimen.

For a more detailed description of the interface element technology for simulating crack growth between independently modeled finite element subdomains, see Pantano and Averill (2002b).

5. Mixed Mode Failure

In defining the softening model, the following properties are needed: the interlaminar tensile and shear strengths T and S, the penalty parameter γ, and the critical strain energy release rates G_{Ic} and G_{IIc}. For simplicity, we assume herein that material behavior is the same for both tensile and compressive loading.

At a given load increment the finite element solution allows us to compute δ_x and δ_z for an interval of the interface element. We also know:

$$\delta_{z0} = \frac{T}{\gamma} \tag{14}$$

$$\delta_{x0} = \frac{S}{\gamma} \tag{15}$$

$$\sigma_z = \gamma \delta_z \tag{16}$$

$$\tau_{xz} = \gamma \delta_x \tag{17}$$

A quadratic interface failure criterion can be written in the following forms:

$$\left(\frac{\sigma_z}{T}\right)^2 + \left(\frac{\tau_{xz}}{S}\right)^2 = 1 \tag{18}$$

$$\left(\frac{\delta_z}{\delta_{z0}}\right)^2 + \left(\frac{\delta_x}{\delta_{x0}}\right)^2 = 1 \tag{19}$$

If the condition in (19) is not satisfied, no action needs to be taken. Otherwise, we assume the following ratio:

$$\frac{\left(\frac{\delta_z}{\delta_{z0}}\right)}{\left(\frac{\delta_x}{\delta_{x0}}\right)} = C_1 \tag{20}$$

to be the same as it was when the failure condition (19) was satisfied first (see Figure 5).

If the load steps are small, then the assumption should be valid. Then, from geometry, it is possible to determine the value of the relative displacements δ_x'and δ_z' corresponding to point F in Figure 5.

$$\delta_x' = \delta_{x0} \frac{\left(\frac{\delta_x}{\delta_{x0}}\right)}{\sqrt{\left(\frac{\delta_z}{\delta_{z0}}\right)^2 + \left(\frac{\delta_x}{\delta_{x0}}\right)^2}} \tag{21}$$

$$\delta_z' = \delta_{z0} \frac{\left(\frac{\delta_z}{\delta_{z0}}\right)}{\sqrt{\left(\frac{\delta_z}{\delta_{z0}}\right)^2 + \left(\frac{\delta_x}{\delta_{x0}}\right)^2}} \tag{22}$$

The interfacial constitutive models are updated for both delamination modes I and II by setting δ_{x0}'=δ_x' and δ_{z0}'=δ_z' (see Figures 6 and 7).

The interlayer tensile strengths T and S are updated accordingly:

$$T' = \gamma_z \cdot \delta'_{z0} \tag{23}$$

$$S' = \gamma_x \cdot \delta'_{x0} \tag{24}$$

Note that the following inequalities hold.

$$\delta_{x0}' \le \delta_{x0}\ ,\quad \delta_{z0}' \le \delta_{z0}\ ,\quad \delta_x \ge \delta_{x0}'\ ,\quad \delta_z \ge \delta_{z0}' \tag{25}$$

The quadratic interaction criterion predicts final failure to be reached when the following condition is satisfied:

$$\left(\frac{G_I}{G_{Ic}}\right)^2+\left(\frac{G_{II}}{G_{IIc}}\right)^2=1 \tag{26}$$

In a similar manner as before, we assume the ratio between (G_{II}/G_{IIc}) and (G_I/G_{Ic}) does not vary as the work of separation grows, as shown in Figure 8:

$$\frac{\left(\frac{G_{II}}{G_{IIc}}\right)}{\left(\frac{G_I}{G_{Ic}}\right)}=C_2 \tag{27}$$

Research on the specimens commonly used for delamination studies shows that, for a given configuration (geometry and loads), the ratio between the strain energy release rates for modes I and II, G_I/G_{II}, does not change appreciably during the entire test (e.g. Choi et al., 1999). This fact provides a valid foundation to our assumption. Thus, it is possible to determine the value of the strain energy release rate G_I' and G_{II}' corresponding to point F in Figure 8.

From geometry it is possible to determine the value of the $(G_I/G_{Ic})'$ at F.

$$G_I'=G_{Ic}\frac{\left(\frac{G_I}{G_{Ic}}\right)}{\sqrt{\left(\frac{G_I}{G_{Ic}}\right)^2+\left(\frac{G_{II}}{G_{IIc}}\right)^2}} \tag{28}$$

In order to evaluate this expression we need to determine (G_I/G_{Ic}), (actual value of G_I divided by G_{Ic}), see Figure 9.

$$G_{Ic}=\frac{T'\cdot\delta_{zF}'}{2}=\frac{\delta_{z0}'\cdot\gamma_z\cdot\delta_{zF}'}{2} \tag{29}$$

$$G_I=G_{Ic}-(\text{Area Triangle}\,OBK)=\frac{\delta_{z0}'\cdot\gamma_z\cdot\delta_{zF}'}{2}-\frac{\left[\delta_z(1-D_z)\gamma_z\right]\cdot\delta_{zF}'}{2} \tag{30}$$

$$\left(\frac{G_I}{G_{Ic}}\right)=\frac{\frac{\delta_{z0}'\cdot\gamma_z\cdot\delta_{zF}'}{2}-\frac{\left[\delta_z(1-D_z)\gamma_z\right]\cdot\delta_{zF}'}{2}}{\frac{\delta_{z0}'\cdot\gamma_z\cdot\delta_{zF}'}{2}}=1-\frac{\delta_z}{\delta_{z0}'}(1-D_z) \tag{31}$$

Similarly, we have:

$$\left(\frac{G_{II}}{G_{IIc}}\right)=\frac{\frac{\delta_{x0}'\cdot\gamma_x\cdot\delta_{xF}'}{2}-\frac{\left[\delta_x(1-D_x)\gamma_x\right]\cdot\delta_{xF}'}{2}}{\frac{\delta_{x0}'\cdot\gamma_x\cdot\delta_{xF}'}{2}}=1-\frac{\delta_x}{\delta_{x0}'}(1-D_x) \tag{32}$$

Now, the updated state of the interfacial constitutive models can be completed for both modes I and II by setting $G_{Ic}' = G_I'$and $G_{IIc}' = G_{II}'$.

Figures 9 and 10 show the final form of the interfacial constitutive models. As can be noticed, the models have different penalty and damage parameters. In this a way, the maximum freedom is allowed for modeling delamination modes I and II.

6. Friction Model

6.1 Evaluation of the force at the interface

It is known that the Lagrange multiplier λ is related to the penalty parameter γ by:

$$F=\lambda=\gamma\cdot\int_s(v-u)\,ds \tag{33}$$

Where F is the force per unit length required to hold the two regions together. It is important to notice that we are not restricted to compute the force on the entire interface, but rather it can be evaluated for a portion of the interface length. This can be performed by changing the extreme values of the interval of integration.

Finally, computation of the interface force does not depend on the compatibility of the interface meshes. Even if the discretizations of the adjacent layers, or layer and skin-stiffener, are different we are still able to choose at will the interface length along which to evaluate forces.

6.2 Implementation of Friction in the Interface Element

The friction model can be applied to interface elements after complete failure or to interface elements whose only purpose is to avoid overlapping and to enforce friction.

For each of the intervals in the interface, the normal force F_n at the interface can be calculated in terms of the normal relative displacement δ_n :

$$F_n=\frac{1}{2}\gamma_n\int_s\delta_n\,ds \tag{34}$$

Assuming Coulomb friction, the tangential force F_t that the interface element needs to generate to simulate the friction phenomenon is:

$$F_t = \frac{1}{2}\gamma_t (1 - D_t) \int_s \delta_t ds = \tau F_n \tag{35}$$

where τ is the friction coefficient and δ_t is the tangential relative displacement. The parameter D_t, which before failure was used as a damage parameter, is now employed as a scale factor able to reduce the value of the penalty parameter for the tangential DOF. Assuming the value of D_t that makes the equality (35) to hold true, the right amount of friction will be generated by the interface element.

The required damage parameter D_t^* related to the tangential relative displacement δ_t can be determined from the following relation:

$$D_t^* = 1 - \frac{2\tau F_n}{\gamma_t \int_s \delta_t ds} \tag{36}$$

6.3 Numerical Test of the Friction Model

A simple test has been performed to verify the reliability and the accuracy of the friction model implemented into the interface element.

The loading, the boundary conditions and the geometry for the test problem are illustrated in Figure 11. Two finite element meshes are connected along the common boundary using one interface element. All the finite elements are rigid and their thickness is 0.5m.

During a quasi-static analysis of 400 load increments, a 1mm tangential displacement is gradually imposed to the nodes of the upper mesh, as shown. At the same time, a pressure load of 1 MPa is applied to the top the upper mesh and is kept constant through the entire analysis. According to the Coulomb law $F_t = \tau \cdot N$, since a coefficient of friction equal to $\tau = 0.1$ is assumed and the contact area is 1 m^2, as expected total reaction force at the interface nodes is:

$$F_t = \tau F_n = \tau \sigma A = 0.1 \cdot 1.e6 \frac{N}{m^2} \cdot 1.m^2 = 1.e5N \tag{37}$$

In the Figure 12 is reported the reaction forces versus the tangential displacement produced by the FE analysis for the interface nodes 1, 2 and 3. For each of the 400 increments in the displacement value, the reaction force at the central node is recorded to be a constant value of 0.5e5N while on the other two nodes a constant value of 0.5e5N is obtained. These sum to the analytical value of 1.e5 N.

7. NUMERICAL RESULTS

7.1 Double Cantilever Beam Test #1

The loading, the boundary conditions and the geometry for the double cantilever beam DCB specimen are illustrated in Figure 13. The DCB test is recognized as pure mode I test. The properties assumed for the beam material are: E_{11}=130 GPa, E_{22}= E_{33} = 8 GPa, G_{12} = 6 GPa, ν= 0.27. The properties of the DCB specimen interface are: G_{Ic} = 257 N/m and σ_i = 20 MPa.

Three finite element models of varying mesh refinement (120x2, 300x8, 600x8) have been used to verify the capabilities of the present approach. In Figure 14, original and deformed models of the DCB test specimen are shown for the coarsest mesh. Two independent meshes compose the finite element models of the upper and lower part of the beam; they are joined by several interface elements. Each interface element connects four finite elements: two on the bottom mesh and two on the top. Experimental results used to validate the present delamination approach have been reported by Chen et al. (1999). A plot of the reaction force as a function of the applied end displacement is shown in Figure 15. Results from the experiment are compared to analytical ones for all the finite element models.

Note that the total number of elements in the meshes is indicated, for example two 120x1 meshes joined by interface elements compose the 120x2 mesh. The predictions from the 120x2 mesh contain many local "bumps". Mi et al. (1999) have analyzed this phenomenon, concluding that coarse meshes can induce these "false instabilities". As the mesh is refined, the predicted response agrees very well with that measured experimentally.

As discussed previously, the damage technique implemented in our model allows portions of the interface, intervals, much smaller than the finite element length, to be released. In Figure 16 convergence of the solution with the number of intervals is investigated for the 300x8 mesh. It can be noticed that as the number of intervals increases the accuracy of the results improves. Figure 17 illustrates the model behavior as a function of the number of increments for the 300x8 mesh. Convergence of the solution to the experimental one is achieved by increasing number of intervals.

7.2 Double Cantilever Beam Test #2

To further verify the ability of the interface to accurately simulate delamination growth in composite materials, a second double cantilever beam DCB test was performed. Material data and experimental results are taken from a different source (Alfano et al., 2001) with respect to the first DCB test.

The loading, the boundary conditions and the geometry for the double cantilever beam DCB specimen are illustrated in Figure 18. The properties assumed for the beam material are: E_{11}=126 GPa, E_{22}=E_{33}=7.5 GPa, G_{12}=4.981 GPa, ν=0.281. The properties of the DCB specimen interface are: G_{Ic} = 263 N/m and σ_i = 57 MPa.

A plot of the reaction force as a function of the applied end displacement is shown in Figure 19. The finite element model has a mesh of 300x8 elements and the displacement boundary conditions are applied in 400 increments. The predicted results compare well with the experimental results.

7.3 End-Loaded Split (ELS) Beam Test

To characterize the mode II delamination, shearing mode, the end-loaded split (ELS) specimen is often used. The loading, the boundary conditions and the geometry for the end-loaded split (ELS) specimen are illustrated in Figure 20.

The properties assumed for the beam material are: E_{11}=130 GPa, E_{22}= E_{33} = 8 GPa, G_{12} = 6 GPa, ν= 0.27. The properties of the ELS specimen interface are: G_{IIc} = 856 N/m and σ_i = 48 MPa. As in the DCB test specimen models, two meshes compose the finite element models of the ELS specimen; they are joined by several interface elements. For the results shown, a 300x8 finite element mesh has been utilized.

In Figure 21, original and deformed models of the ELS test specimen are shown. Experimental results used to validate the present delamination approach have been reported by Chen et al. (1999). A plot of the reaction force as function of the applied end displacement is shown in Figure 22. Convergence of the solution as the number of increments increases is demonstrated. The comparison with experimental results is again very good.

7.4 Fixed-Ratio Mixed Mode (FRMM) Test

To test the mixed mode I+II delamination capabilities of the interface model, the Fixed-Ratio Mixed Mode (FRMM) specimen has been considered. The loading, the boundary conditions and the geometry for the FRMM specimen are illustrated in Figure 23.

The properties assumed for the beam material are: E_{11}=130 GPa, E_{22}= E_{33} = 8 GPa, G_{12} = 6 GPa, ν= 0.27. The properties of the ELS specimen interface are: G_{Ic} = 257N/m, G_{IIc} = 856N/m and σ_i = 48 MPa. As in the DCB and ELS test specimens models, two meshes compose the finite element models of the ELS specimen; they are joined by several interface elements. For the results shown, a 300x8 finite element mesh has been utilized.

In Figure 24, original and deformed models of the ELS test specimen are shown. Experimental results used to validate the present delamination approach have been reported by Chen et al. (1999). A plot of the reaction force as function of the applied end displacement is shown in Figure 25. The predictions agree well with the experimental results, demonstrating that the novel mixed mode damage model implemented in the interface element is able to correctly predict delamination growth in a mixed mode FE simulation.

8. CONCLUSIONS

A new interface element technology has been presented for predicting crack growth in laminated structures. This interface method is capable of joining and simulating crack growth between independently modeled finite element subdomains (e.g., composite plies). The interface element approach makes it possible to release sub-regions of the interface surface whose length is smaller than that of the finite elements, thereby allowing for a mesh-independent tracking of the crack front. A novel approach for modeling the crack growth in mixed mode I+II conditions has been developed. Results for double cantilever beam DCB, end-loaded split (ELS) and fixed-ratio mixed mode (FRMM) specimens indicate that the method is capable of accurately predicting delamination growth.

9. ACKNOWLEDGMENTS

This work was sponsored by NASA Langley Research Center under grant NAG-1-2213. The authors are grateful for the helpful comments of Dr. Jonathan Ransom and Carlos Davila. Partial support was also provided by the State of Michigan Research Excellence Fund.

10. REFERENCES

[1] Alfano, G., Crisfield, M.A., 2001. Finite element interface models for the delamination analysis of laminated composites: mechanical and computational issues. International Journal for Numerical Methods in Engineering 50, 1701-1736.

[2] Allix, O., Corigliano, A., 1999. Geometrical and interfacial non-linearities in the analysis of delamination in composites. International Journal of Solids and Structures 36, 2189-2216.

[3] Aminpour, M.A., Hosapple, K.A, 1991. Finite element solutions for propagating interface crack with singularity elements. Engineering Fracture Mechanics 39 (3), 451-468.

[4] Aminpour, M.A., Krishnamurthy, T., 1997. A Two-Dimensional Interface Element for Multi-Domain Analysis of Independently Modeled Three-Dimensional Finite Element Meshes. AIAA paper 97-1297, 1853-1861.

[5] Aminpour, M.A., Krishnamurthy, T., Fadale, T.D., 1998. Coupling of Independently Modeled Three-Dimensional Finite Element Meshes with Arbitrary Shape Interface Boundaries. AIAA paper 98-2060, 3014-3024.

[6] Aminpour, M.A., Pageau, S., Shin, Y., 2000. An Alternative Method for the Interface Modeling Technology. AIAA paper 2000-1352, 1-13.

[7] Aminpour, M.A., Ransom, J.B., McCleary, S.L., 1995. A Coupled Analysis Method for Structures with Independently Modeled Finite Element Subdomains. International Journal for Numerical Methods in Engineering 38, 3695-3718.

[8] Bottega, W.J., 1983. A growth law for propagation of arbitrary shaped delaminations in layered plates. International Journal of Solids and Structures 19 (11), 1009-1017.

[9] Chakraborty, D., Pradhan, B., 1999. Effect of ply thickness and fiber orientation on delamination initiation in broken ply composite laminate. Journal of Reinforced Plastic and Composites 18 (8), 735-758.

[10] Chang, F., Springer, G.S., 1986. Strength of fiber reinforced composite bends. Journal of Composite Materials 20, 30-45.

[11] Chen, J., Crisfield, M., Kinloch, A.J., Busso, E.P., Mattehws, F. L., Qiu, Y., 1999. Predicting Progressive Delamination of Composite Materials Specimens via Interface Elements. Mechanics of Composite Materials and Structures 6, 301-317.

[12] Cho, M., Kim, W.B, 1998. A Coupled Finite Element Analysis of Independently Modeled Substructures by Penalty Frame Method. AIAA paper 98-2061, 3025-3032.

[13] Choi, N.S., Kinloch, A.J., Williams, J.G., 1999. Delamination fracture of multidirectional carbon-fiber/epoxy composites under mode I, mode II and mixed-mode I/II loading. Journal of Composite Materials 33, 73-101.

[14] Dakshima Moorthy, C..M., Reddy, J.N., 1999. Recovery of Interlaminar Stresses and Strain Energy Release Rates in Composite Laminates. Finite Elements in Analysis and Design 33, 1-27.

[15] Davila, C., Camanho, P., de Moura, M.F., 2001. Mixed-Mode Decohesion Elements for Analyses of Progressive Delamination. 42nd AIAA/ASME/ASCE/AHS/ASC Structural Dynamics and Materials Conference, Seattle, Washington, paper AIAA-01-1486.

[16] Farhat, C., Gerardin, M., 1992. Using a reduced number of Lagrange multipliers for assembling parallel incomplete field finite element approximations. Computer Methods in Applied Mechanics and Engineering 97, 333-354.

[17] Farhat, C., Roux, F.X., 1991. A method of finite element tearing and interconnecting and its parallel solution algorithm. International Journal for Numerical Methods in Engineering 32, 1205-1227.

[18] Hitchings, D., Robinson, P., Javidrad, F., 1996. Finite Element Model for Delamination Propagation Composites. Computers & Structures 60 (6), 1093-1104.

[19] Housner, J.M., Aminpour, M.A., Davila, C.G., Schiermeier, J.E., Stroud, W.F., Ransom, J.B., Gillian, R.E., 1995. An Interface Element for Global/Local and Substructuring Analysis. MSC World Users' Conference, Los Angeles, CA, May 8-12.

[20] Hwu, C., Kao, C.J., Chang, L.E., 1995. Delamination fracture criteria for composite laminates. Journal of Composite Materials 29 (15), 1962-1987.

[21] Jinping, Z., Huizu, A., 1991. Stress analysis around holes in orthotropic plates by subregion mixed finite element method. Computers & Structures 41 (1), 105-108.

[22] Joo, J.W., Sun, C.T., 1994. Failure criterion for laminates governed by free edge interlaminar shear stress. Journal of Composite Materials 26 (10), 573-586.

[23] Kaczmarek, K., Wisnom, M.R., Jones, M.I., 1998. Edge delamination in curved (0/±45)s glass-fibre/epoxy beams loaded in bending. Composites Science and Technology 58 (1), 155-161.

[24] Ko, C., Lin, C., Chin, H., 1992. Prediction for delamination initiation around holes in symmetric laminates. Composite Structures 22 (4), 87-191.

[25] Ladevèze, P., 1992. A Damage Computational Method for Composite Structures. Computers & Structures 44, 78-87.

[26] Lammerant, L., Verpoest, I., 1996. Modelling of the interaction between matrix cracks and delaminations during impact of composite plates. Composites Science and Technology 56 (10), 1171-1178.

[27] Lee, J., Gao, H., 1995. A hybrid finite element analysis of interface cracks. International Journal for Numerical Methods in Engineering 38, 2465-2482.

[28] Maday, Y., Mavriplis, C., Patera, A., 1988. Non-conforming mortar element methods: Application to spectral discretizations. NASA CR-181729, ICASE Report No. 88-59.

[29] Mi, Y., Crisfield, A., Davies, A.O., Hellweg, H.B., 1998. Progressive Delamination Using Interface Elements. Journal of Composite Materials 32 (14), 1246-1272.

[30] Moes, N., Dolbow, J., Belytschko, T., 1999. A finite element method for crack growth without remeshing. International Journal for Numerical Methods in Engineering 46, 131-150.

[31] Mohammadi, S., Owen, D.R.J., Peric, D., 1998. A Combined Finite/Discrete Element Algorithm for Delamination Analysis of Composites. Finite Elements in Analysis and Design 28, 321-336.

[32] Ortiz, M., Pandolfi, A., 1999. Finite-deformation irreversible cohesive element for three-dimensional crack-propagation analysis. International Journal for Numerical Methods in Engineering 44, 1267-1282.

[33] Pandolfi, A., Krysl, P., Ortiz, M., 1999. Finite element simulation of ring expansion and fragmentation: The capturing of length and time scale through cohesive models of fracture. International Journal of Fracture 95, 279-297.

[34] Pantano, A., Averill, R.C., 2002. A Penalty Based Finite Element Interface Technology. Computers & Structures 80 (22), 1689-1748.

[35] Pantano, A., Averill, R.C., 2002. A penalty-based interface technology for connecting independently modeled substructures and for simulating growth of delamination in composite structures. *PhD Thesis*, Michigan State University, East Lansing, MI, 2002. United States Patent TX 5-644-766 (10 February 2003).

[36] Point, N., Sacco, E., 1996. A Delamination Model for Laminated Composites. International Journal of Solids and Structures 33 (4), 483-509.

[37] Pradhan, S.C., Tay, T.E., 1998. Three-Dimensional Finite Element Modelling of Delamination Growth in Notched Composite Laminates Under Compressive Loading. Engineering Fracture Mechanics 60 (2), 157-171.

[38] Raju, I.S., Sistla, R., Krishnamurthy, T., 1996. Fracture Mechanics Analyses for Skin-Stiffener Debonding, Engineering Fracture Mechanics 54 (3), 371-385.

[39] Ransom, J.B., 1997. Interface Technology for Geometrically Nonlinear Analysis of Multiple Connected Subdomains. AIAA Paper 97-1298.

[40] Ransom, J.B., McCleary, S.L., Aminpour, M.A., 1993. A New Interface Element for Connecting Independently Modeled Substructures. AIAA Paper 93-1503.

[41] Reedy, E.D., Mello, F.J., Guess, T.R., 1997. Modeling the initiation and growth of delaminations in composite structures. Journal of Composite Materials 31 (8), 812-831.

[42] Rinderknecht, S., Kroplin, B., 1997. A computational method for the analysis of delamination growth in composite plates. Computers and Structures 64 (1-4), 359-374.

[43] Schellekens, J.C.J., de Borst, R., 1993. A Non-Linear Finite Element Approach for the Analysis of Mode-I Free Edge Delamination in Composites. International Journal of Solids and Structures 30 (9), 1939-1953.

[44] Schipperen, J.H.A., Lingen, F.J., 1999. Validation of two-dimensional calculation of free-edge dalamination in laminated composites. Composite Structures 45, 233-240.

[45] Wang, J.T., Raju, I.S., 1996. Strain Energy Release Rate Formulae for Skin-Stiffener Debond Modeled with Plate Elements. Engineering Fracture Mechanics 54 (2), 221-228.

[46] Zhao, J., Hoa, S.V., Xiao, X.R., Hanna, I., 1999. Global/Local Approach Using Partial Hybrid Finite Element Analysis of Stress Fields in Laminated Composites with Delamination Under Bending. Journal of Reinforced Plastic and Composites 18 (9), 827-843.

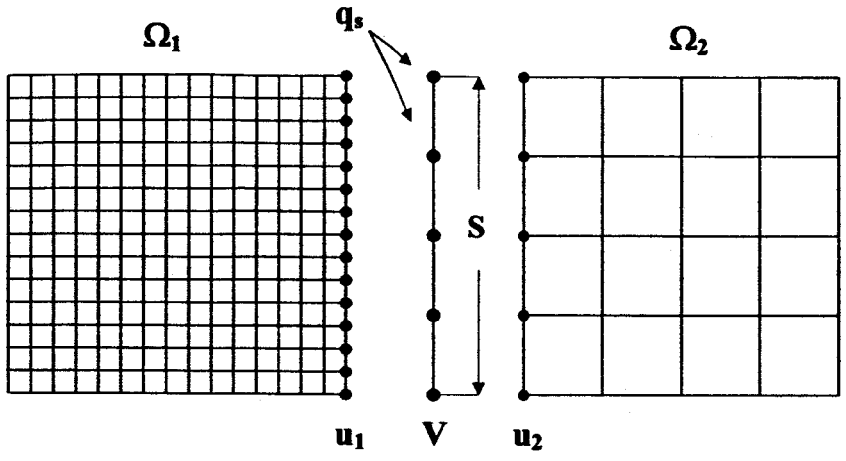

(a)

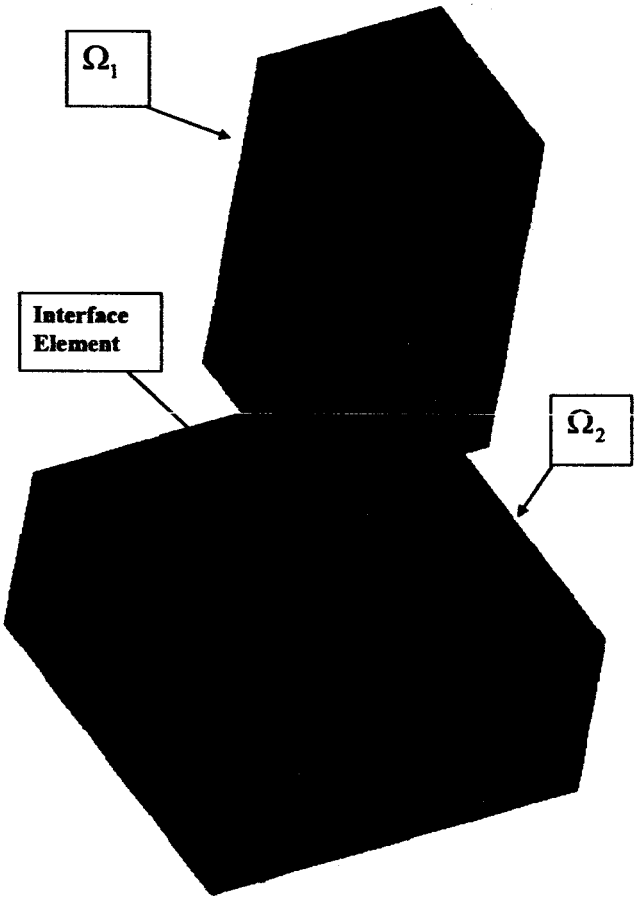

(b)

Figure 1. (a) 2D and (b) 3D Interface element configurations.

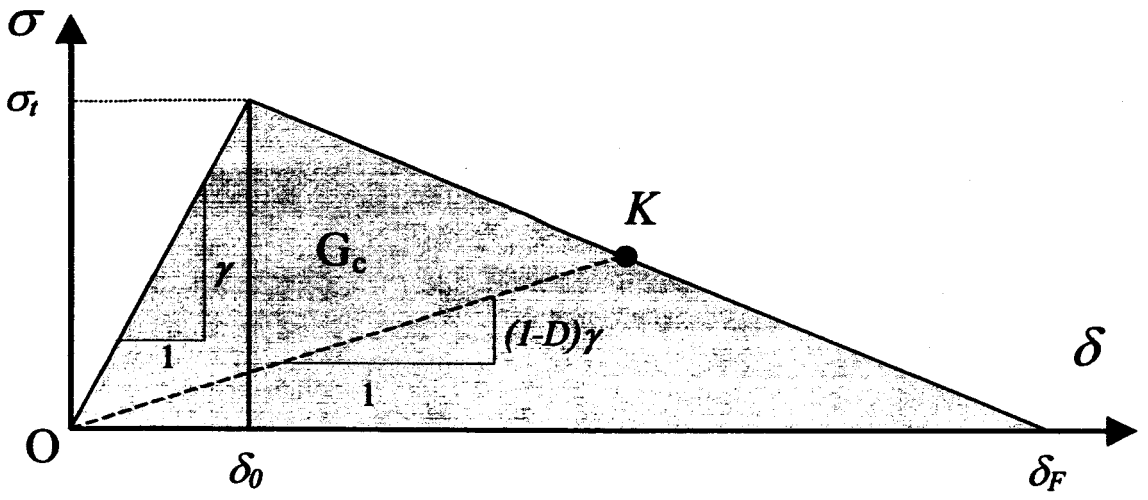

Figure 2. Bilinear interfacial constitutive damage model.

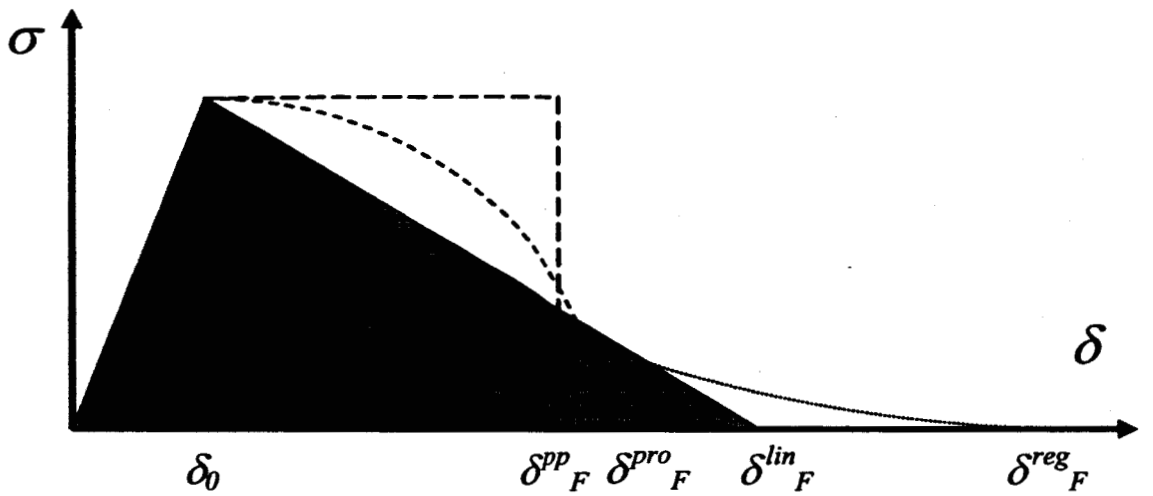

Figure 3. Interfacial constitutive damage models commonly adopted, where *pp* refers to …, *pro* refers to …, *lin* refers to the bilinear model used herein, and *reg* refers to … .

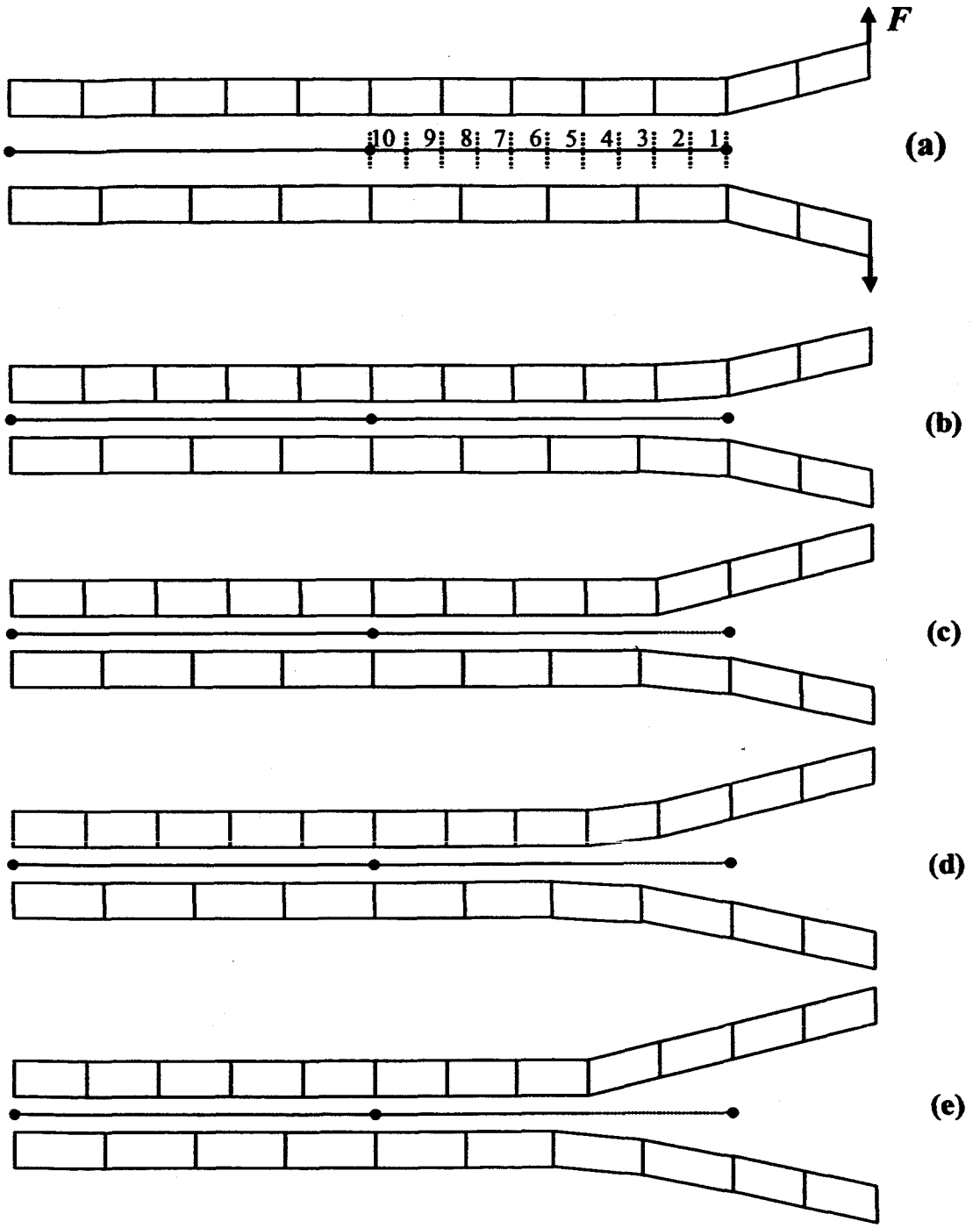

Figure 4. Division of the interface element in intervals

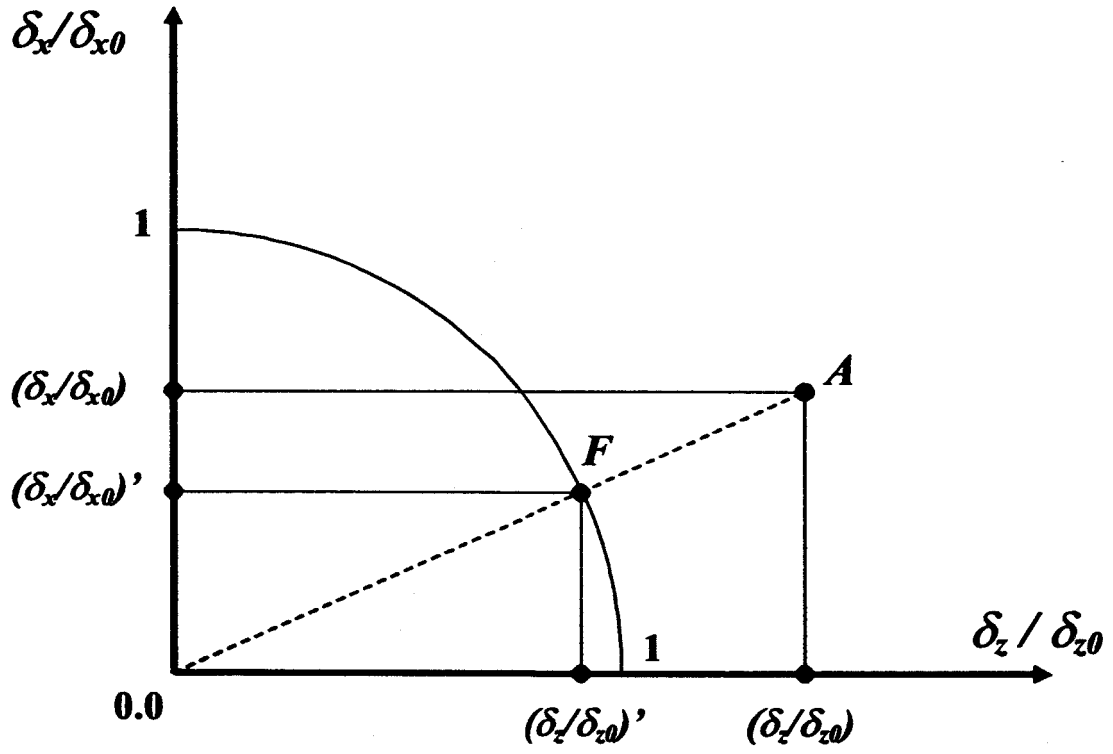

Figure 5. Quadratic failure envelope for tensile-tensile loading.

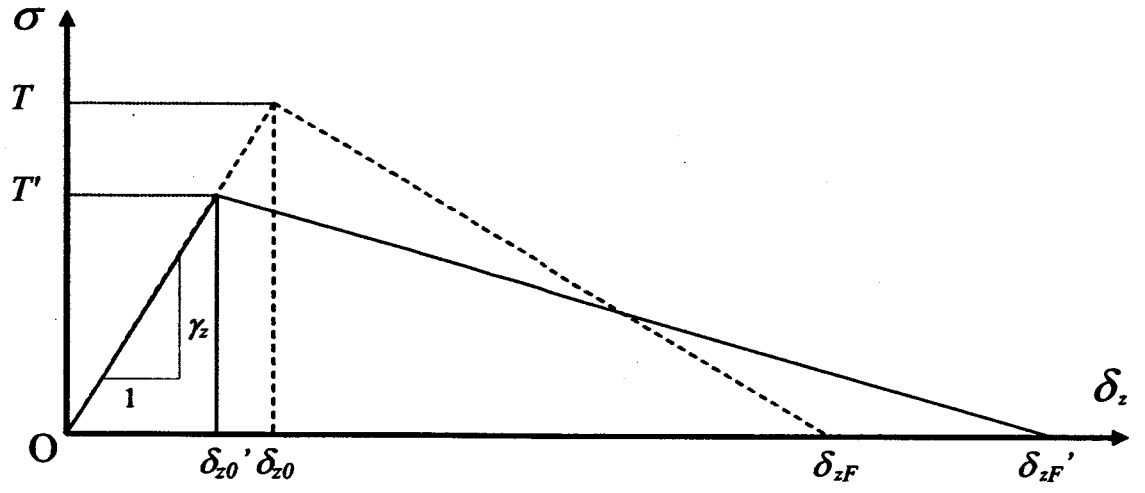

Figure 6. Updated interfacial constitutive model for mode I.

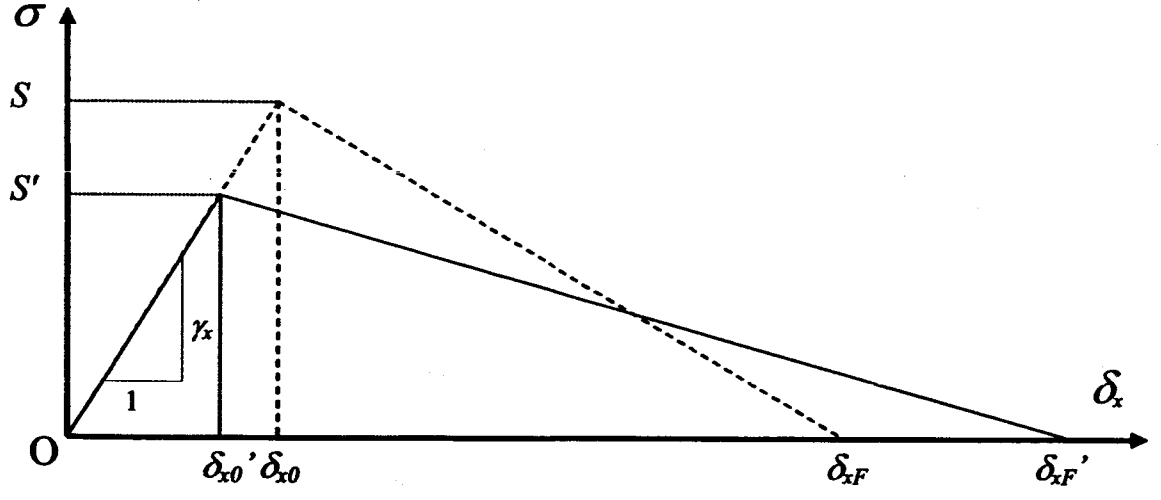

Figure 7. Updated interfacial constitutive model for mode II.

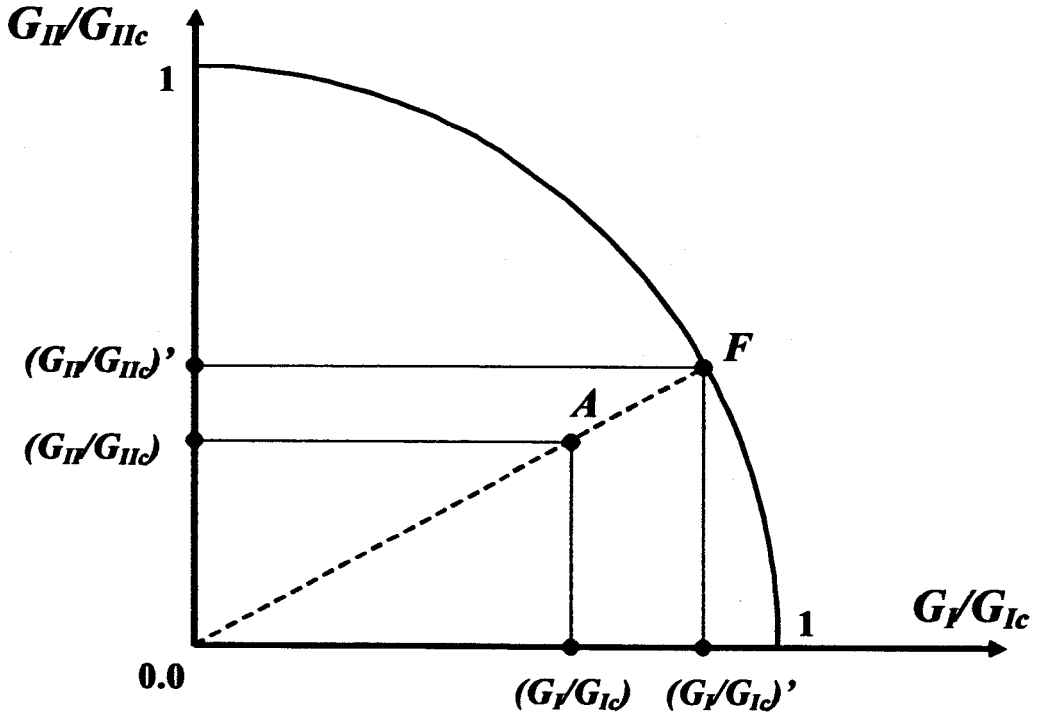

Figure 8. Quadratic final failure surface.

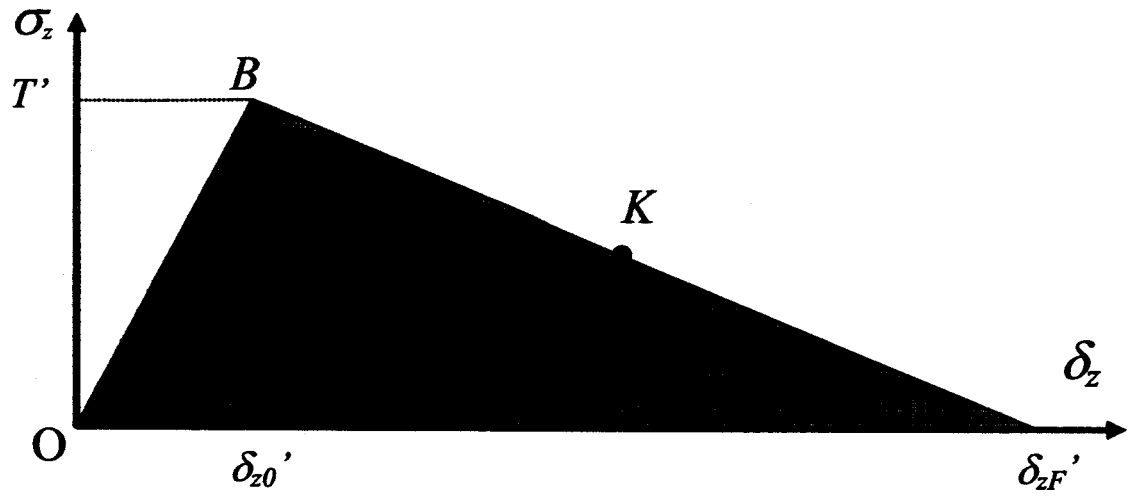

Figure 9. Final interfacial constitutive model for mode I delamination.

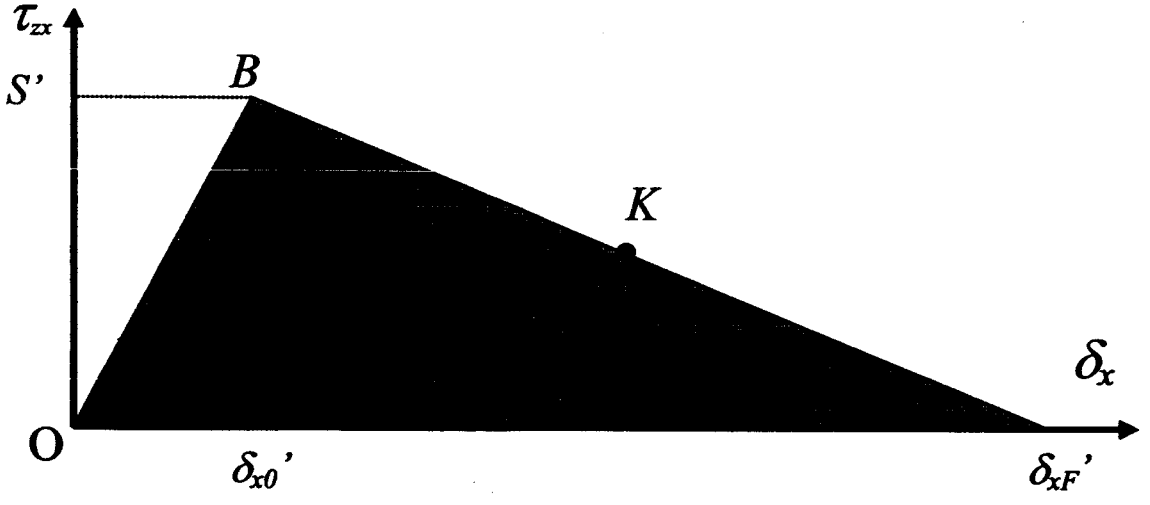

Figure 10. Final interfacial constitutive model for mode II delamination.

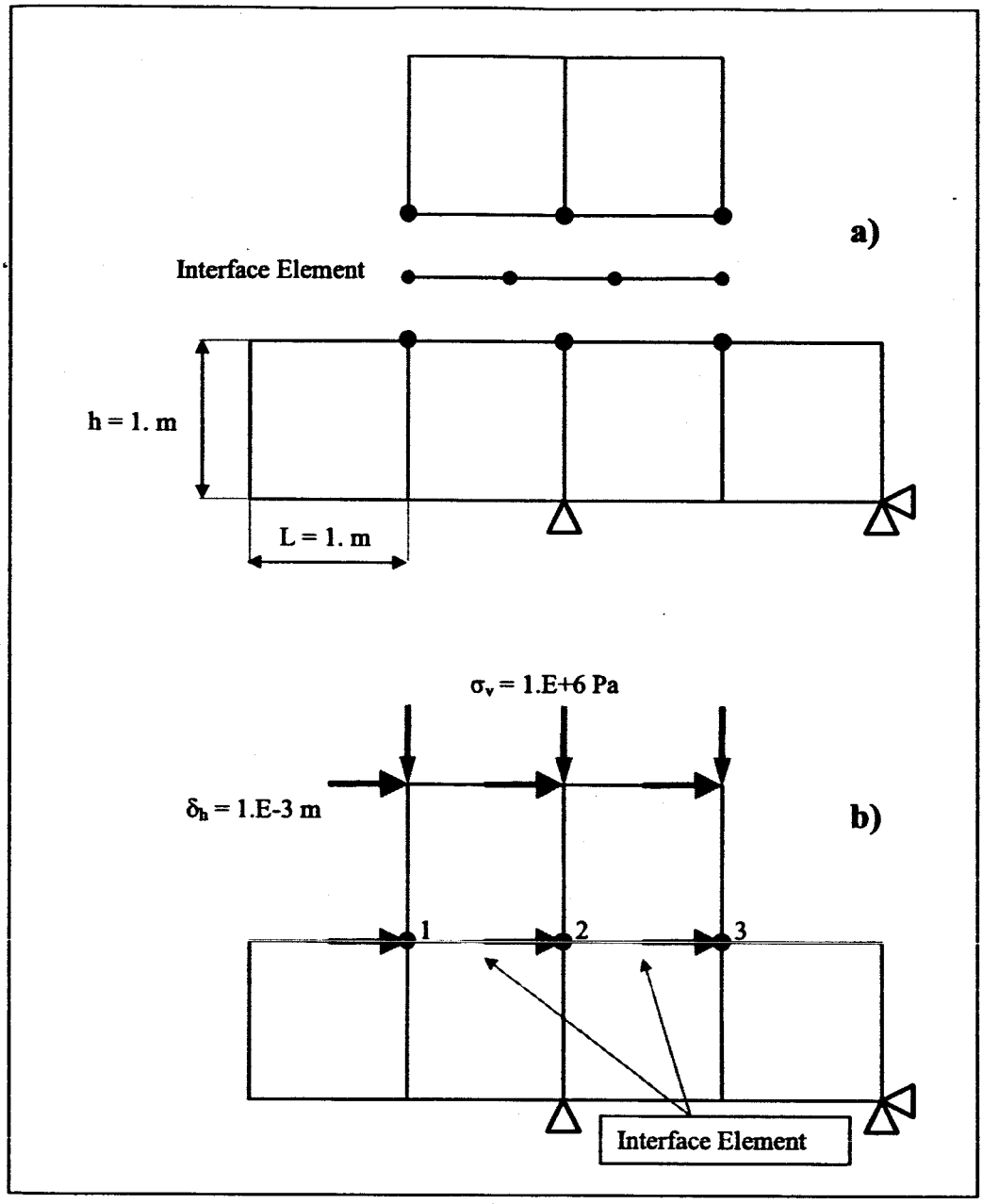

Figure 11. Loading, boundary conditions and geometry for the friction test problem. a) Exploded view, b) assembled view.

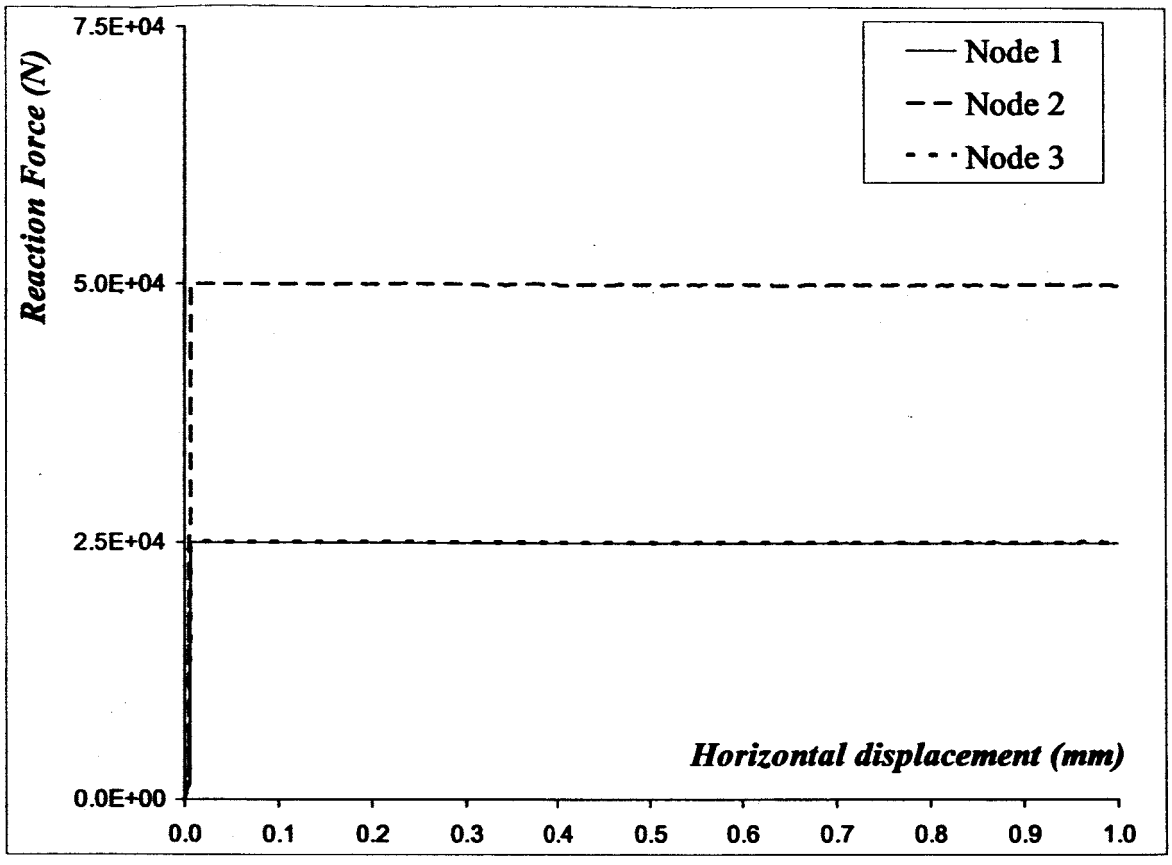

Figure 12. Test Friction – Graph Force-Displacements.

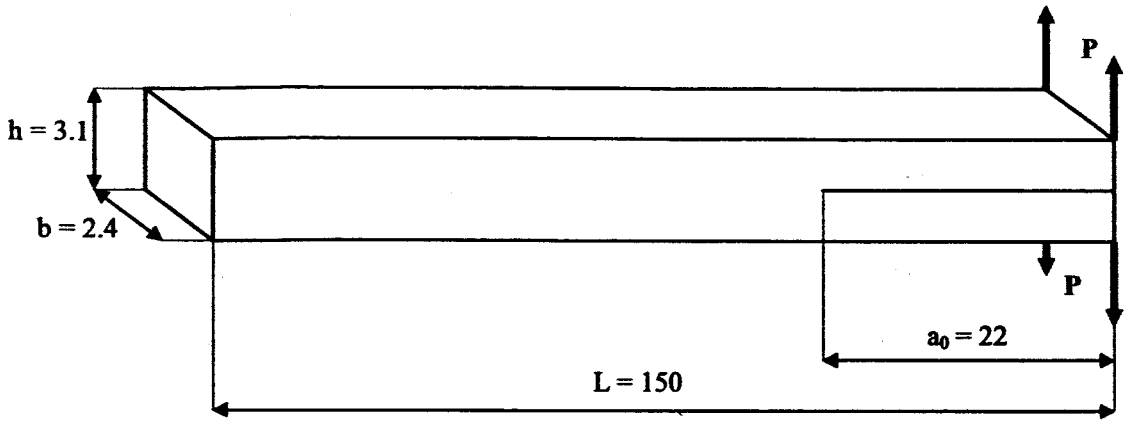

Figure 13. Geometry and boundary conditions for the DCB test specimen.

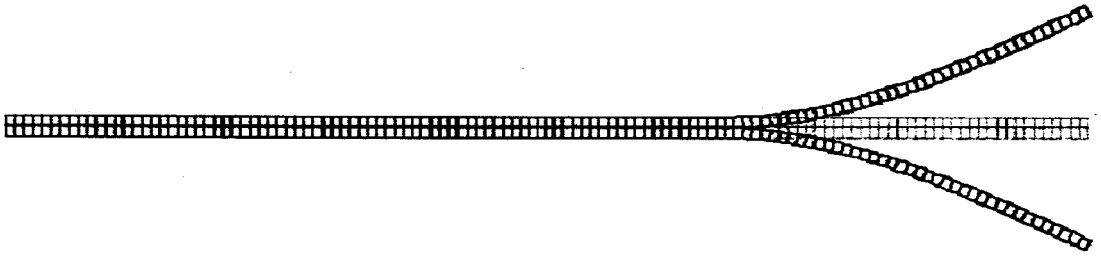

Figure 14. Original and deformed (5mm opening) models of the DCB test specimen using a 120x2 mesh.

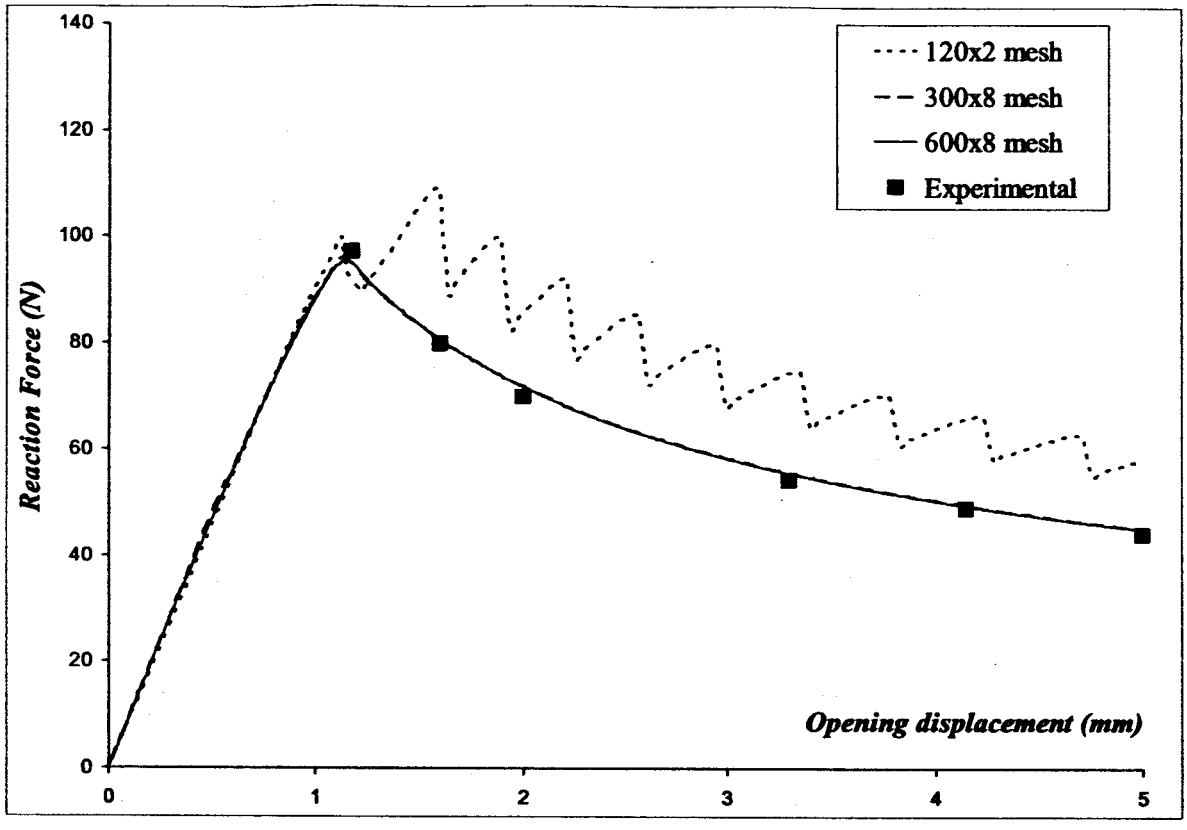

Figure 15. Force vs. displacement results of experimental and numerical DCB test

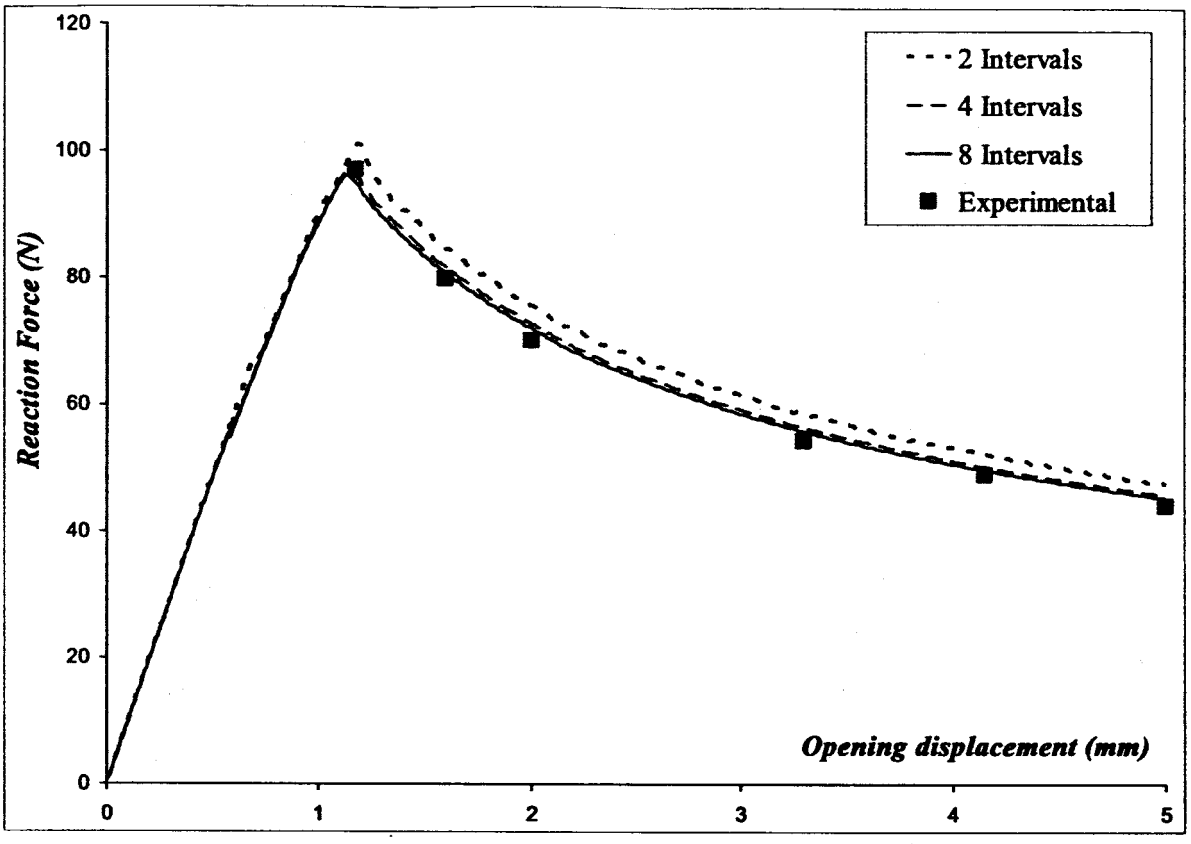

Figure 16. Force vs. displacement results of DCB test. Convergence of the solution with intervals number. Mesh 300x8.

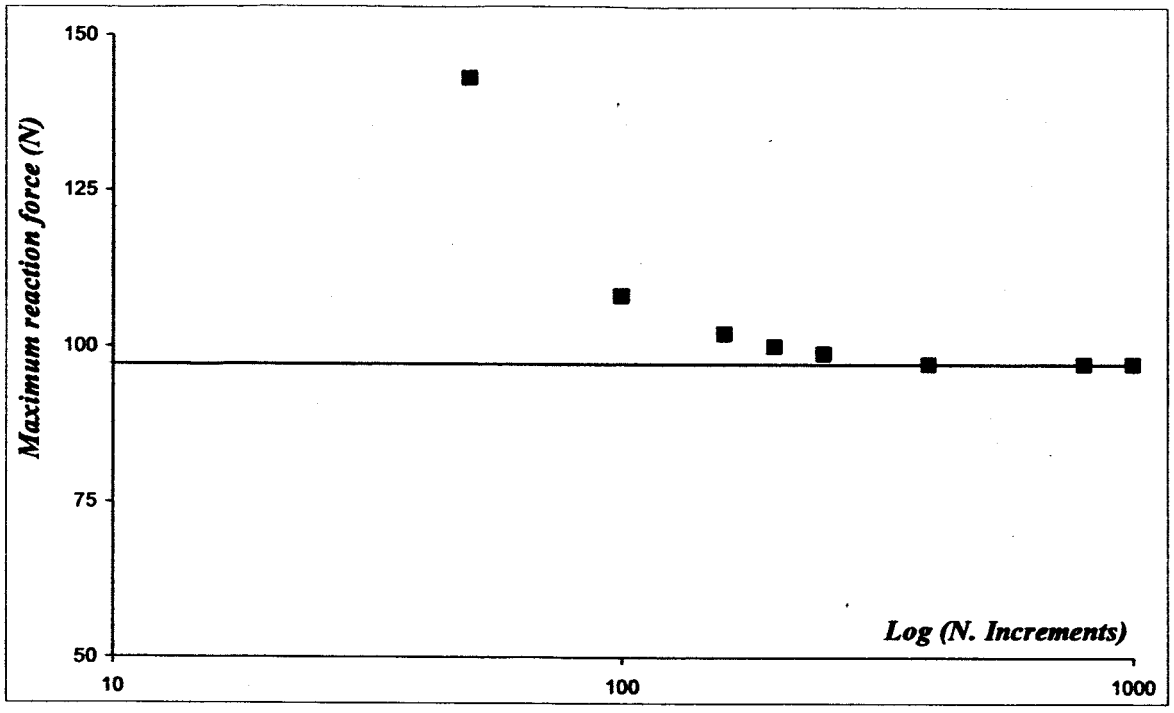

Figure 17. Convergence of the solution with the number of increments. Mesh 300x8.

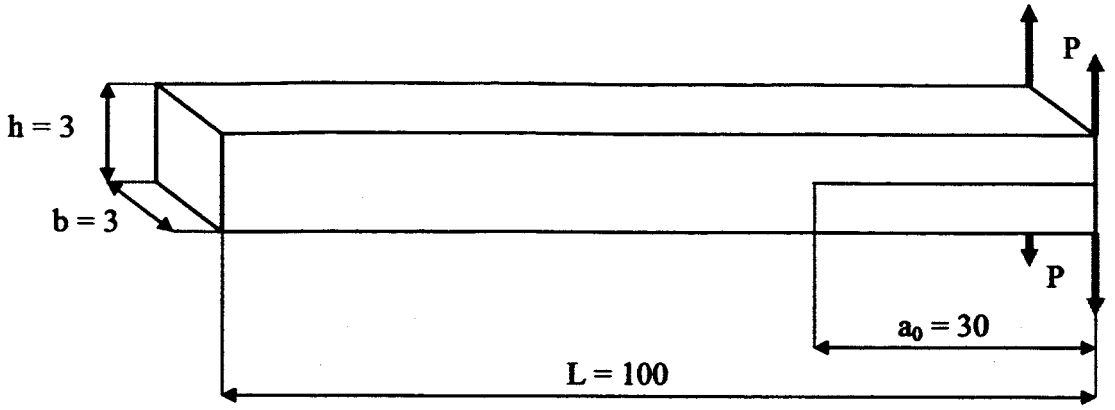

Figure 18. Geometry and boundary conditions for the DCB test #2

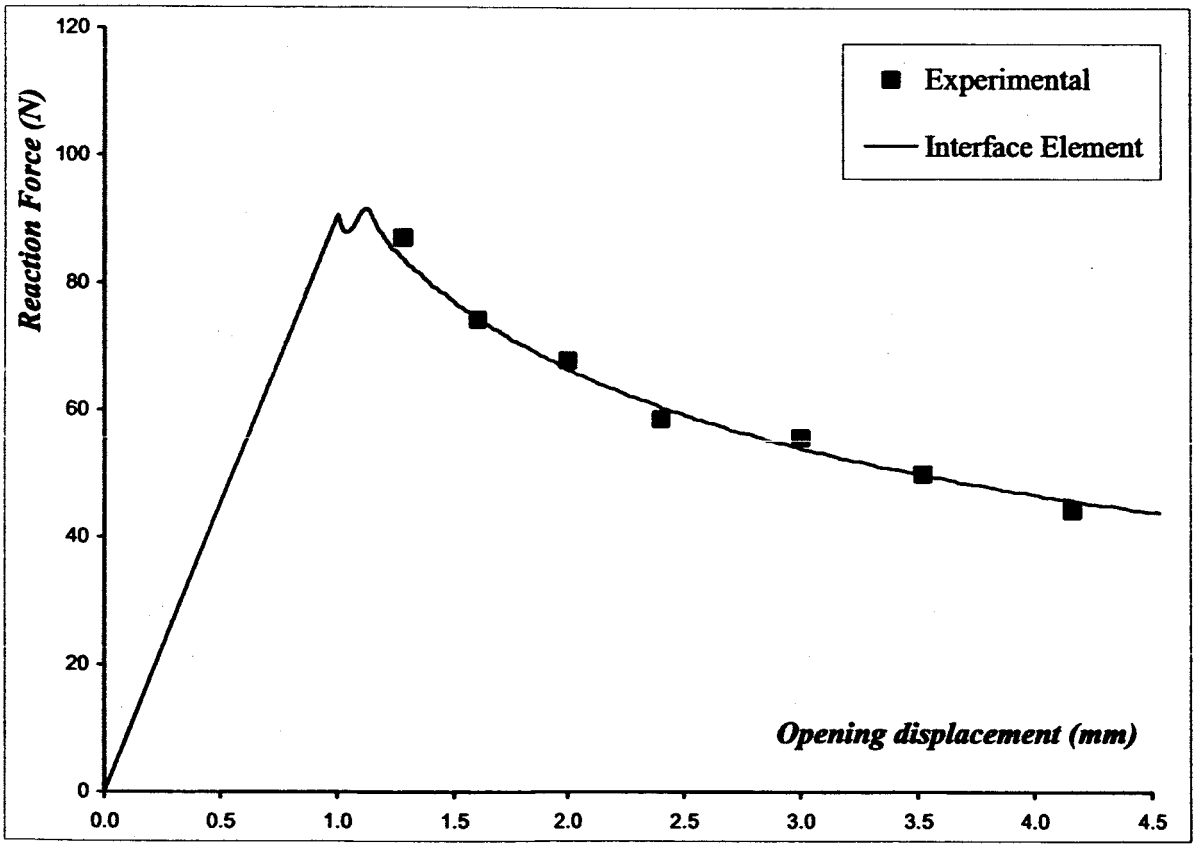

Figure 19. Force vs. displacement results of experimental and numerical DCB test #2

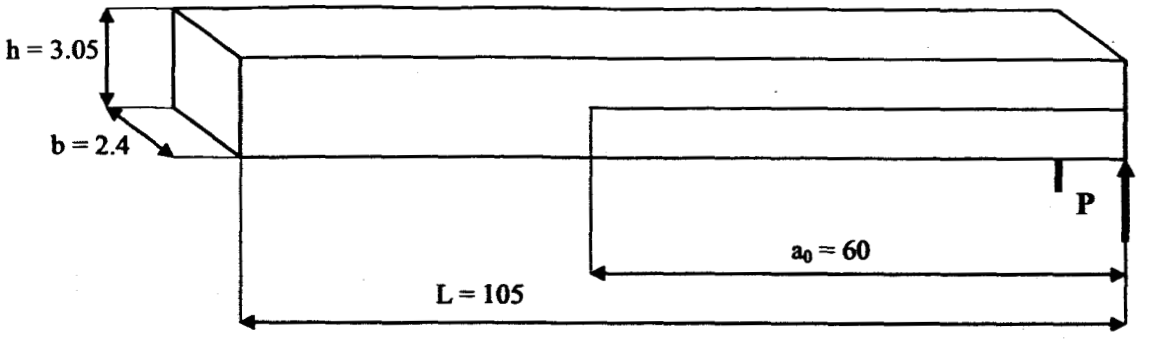

Figure 20. Geometry and boundary conditions for the ELS test specimen.

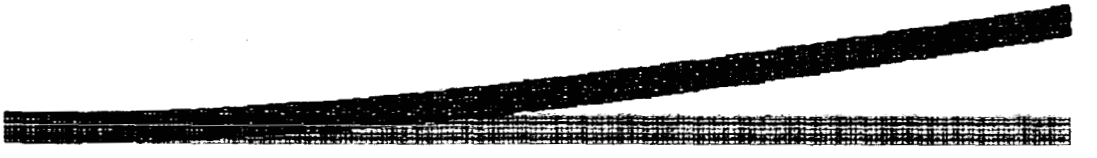

Figure 21. Original and deformed (30mm tip displacement) models of the ELS test specimen for a 300x8 mesh.

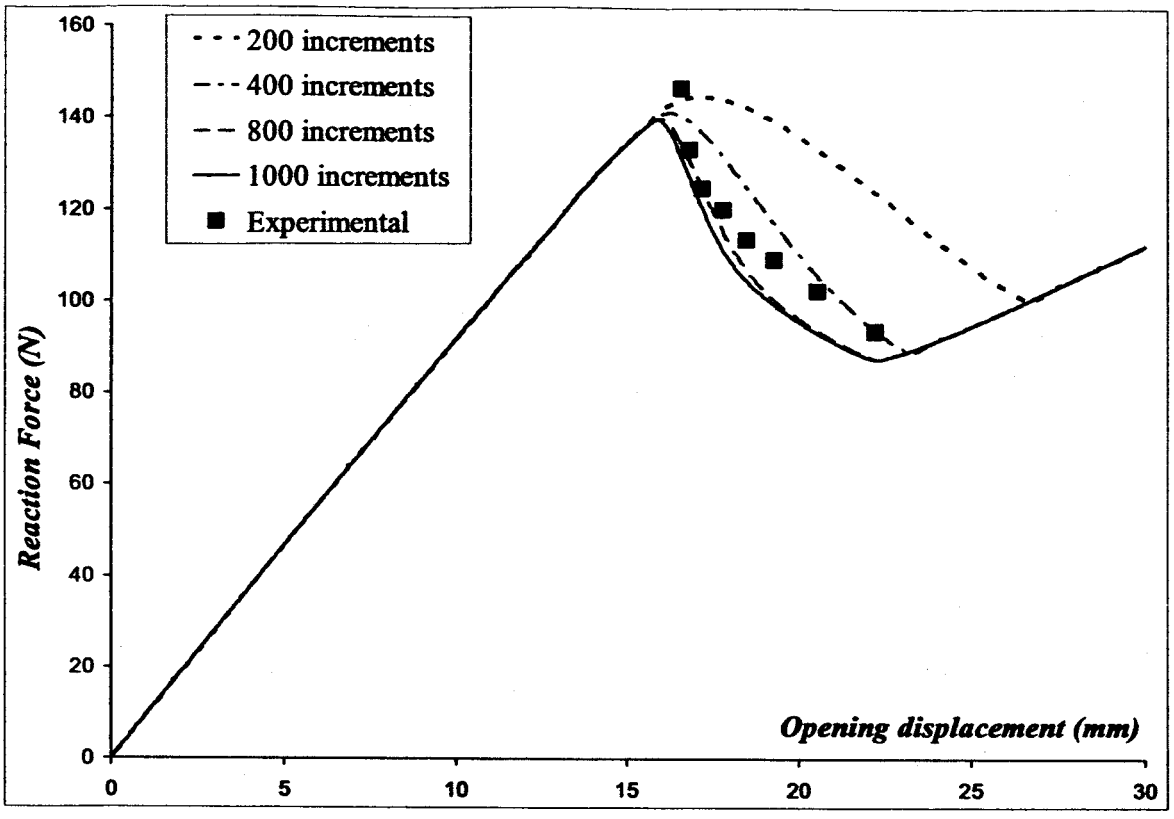

Figure 22. Force vs. displacement results of experimental and analytical ELS test for varying number of loading increments.

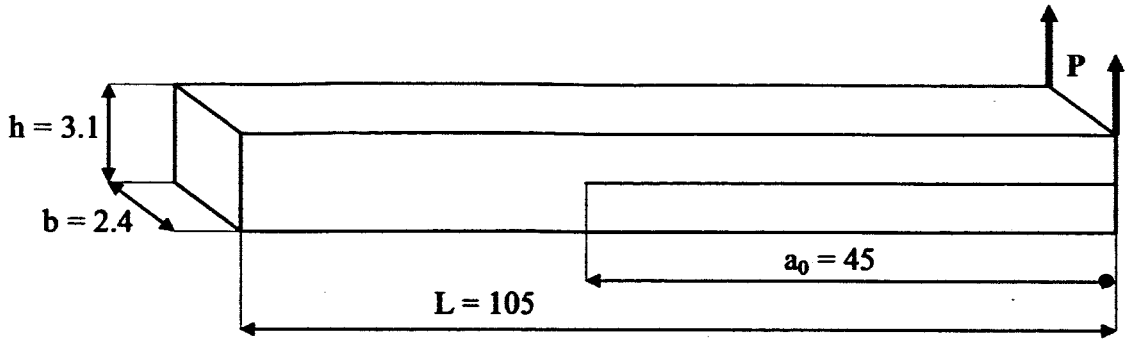

Figure 23. Geometry and boundary conditions for the FRMM test

Figure 24. Original and deformed (20mm tip displacement in absence of delamination) models of the FRMM test specimen.

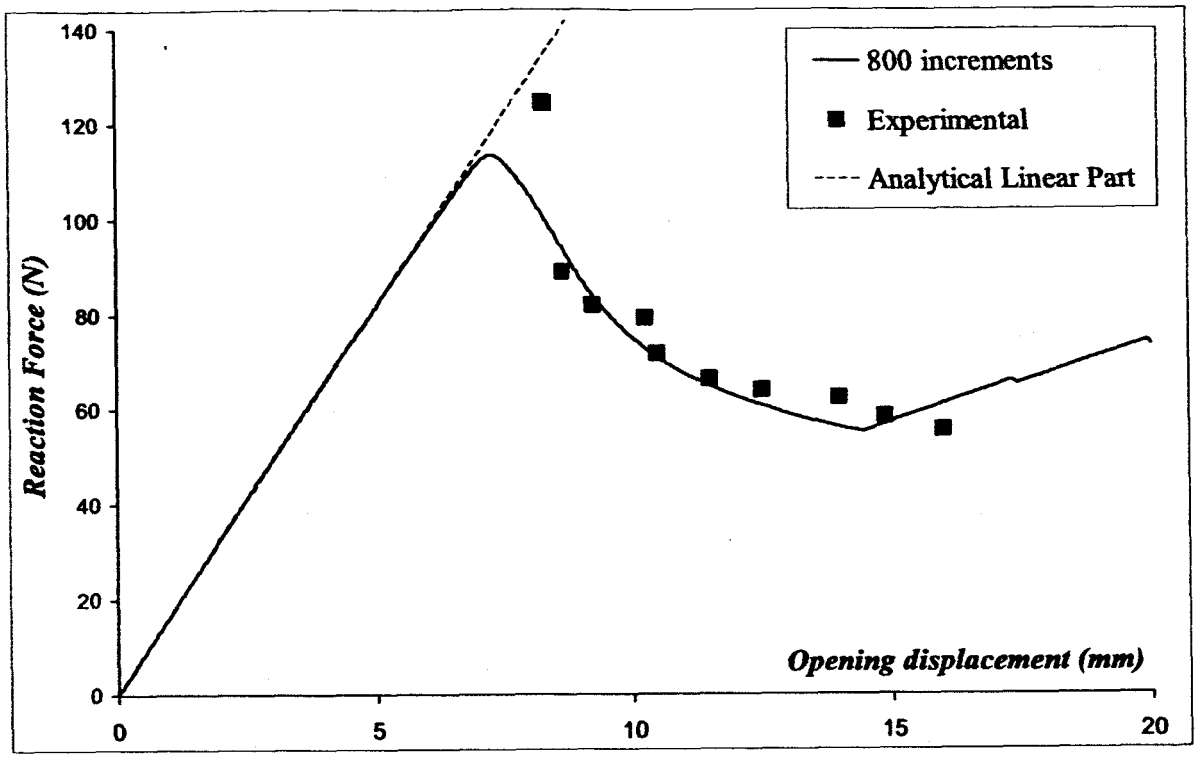

Figure 25. Force vs. displacement results of experimental and numerical FRMM test.